Structure and Orientation of Interfacial Water Determine Atomic Force Microscopy Results: Insights from Molecular Dynamics Simulations

Dimitrios Argyris,[†] Paul D. Ashby,[‡] and Alberto Striolo[†,*]

[†]School of Chemical, Biological, and Materials Engineering, The University of Oklahoma, Norman, Oklahoma 73019, United States and [‡]Molecular Foundry, Materials Science Division, Lawrence Berkeley National Laboratory, Berkeley, California 94720, United States

ABSTRACT Massive all-atom molecular dynamics simulations were employed to study hydration forces near α-Al_2O_3 (0001) surfaces as sampled during a hypothetical AFM force spectroscopy experiment conducted using a (28,0) single-walled carbon nanotube as the tip at ambient conditions. The results provide the force acting on the carbon nanotube tip, as well as detailed properties of interfacial water, as a function of the nanotube−surface distance. As the tip approaches the solid substrate, interfacial water undergoes conformational and structural changes. These changes are responsible for the features observed in the force profiles, including the range at which forces can be measured (up to two hydration shells), the intensity of the forces experienced by the AFM tip, and their oscillatory character. Our detailed analysis shows that heterogeneous surface chemical composition results in appreciably different force profiles. This observation may explain the variability of AFM data sampling hydration forces even on atomically smooth substrates. In addition, our results suggest that sufficiently accurate AFM force spectroscopy could be used to study how hydration forces depend on surface heterogeneous properties and on the orientation and local density of interfacial water, which could aid our understanding of interfacial phenomena and lead to significant scientific breakthroughs.

KEYWORDS: force spectroscopy · alumina · carbon nanotubes · water structure

Interfacial water plays a key role in a number of important phenomena observable in nature including ion adsorption/desorption processes on solid substrates and ion diffusion in biological membranes and ion channels.[1−5] Several molecular-level aspects of water at interfaces have been explored in numerous experimental[6−8] and theoretical[9−14] studies. It has been shown that solid substrates affect structural and dynamical properties of interfacial water, resulting in significantly different behavior compared to that of water in the bulk.[15,16] Probing the properties of hydration water has been the focus of several experimental studies, conducted using a number of techniques including neutron scattering,[17] sum-frequency vibrational spectroscopy,[18] surface force apparatus (SFA),[19] and atomic force microscopy (AFM).[20−22] SFA and AFM yield force profiles between two surfaces or between one surface and the AFM tip, respectively. These force profiles typically show oscillatory behavior with fixed periodicity of roughly the diameter of a water molecule and of increasing amplitude as the separation decreases. Oscillations in the force profiles are believed to occur as water molecules are displaced from discrete interfacial layers. We demonstrate with all-atom molecular dynamics simulations that the density and orientation of interfacial water molecules may lead to force profiles with complex oscillatory character.

Several attempts have been reported using the AFM to sample the properties of interfacial water. For instance, Jarvis *et al.*[20] and Higgins *et al.*[23] reported hydration forces on a self-assembled monolayer and on lipid bilayers, respectively, by utilizing an AFM with tips made by multiwalled carbon nanotubes. Riedo and co-workers[21] sampled the viscosity of water confined between the AFM tip and surfaces of various degrees of hydrophilicity. Loh and Jarvis[24] showed that the AFM, in the frequency modulation mode, can be used to map not only the atomic properties of cleaved muscovite mica but possibly the adsorption of aqueous ions on such surfaces. Even more impressively, Fukuma *et al.* proposed a three-dimensional approach to employ frequency-modulated scanning force microscopy results to visualize in short times three-dimensional force profiles near a solid surface.[25] In this specific example, a mica surface was used, immersed in PBS, and sampled with a silicon tip. The data were interpreted as repulsive forces indicating the presence of hydration water molecules. These and other[19,26−28] experimental reports consistently show oscillatory force profiles as the AFM tip approaches the

* Address correspondence to astriolo@ou.edu.

Received for review December 14, 2010 and accepted February 18, 2011.

Published online March 04, 2011
10.1021/nn103454m

surface, suggesting that the technique could be used to obtain details regarding the hydration layers.[29] Simulation studies have been conducted to aid both planning and interpreting such AFM experiments. For example, Patrick and Lynden-Bell provide molecular insights obtained by means of molecular dynamics simulations on the solvation forces acting on an AFM tip and present force−distance curves for a number of tips configurations.[30] Smaller amplitude oscillations are observed in the force profile for sharper tips. Ho *et al.*[31] employed classical density functional theory to estimate the magnitude and the range of solvation forces as measured by AFM. The results suggest that solvation forces depend on the shape of the AFM tip apex, and that the solvation forces do not extend for distances larger than 2−3 molecular diameters from the substrate. Both experimental and simulation AFM simulation data reported by Riedo and co-workers[21] show oscillatory hydration forces, although with different characteristics depending on the nature of the substrates considered. More recently, Hiasa *et al.*[32] employed frequency-modulated atomic force microscopy to sample the properties of hydration water on α-Al_2O_3 ($01\bar{1}2$). The AFM tip was gold-coated silicon, and the aqueous solution was of 1 M KCl concentration. The force−distance curves reported, once the electric double-layer contribution was subtracted, showed four different types of profiles. The authors interpreted the results with the presence of heterogeneous interfacial water structure on the wafer surface. Even the results by Fukuma *et al.*[25] showed that force−distance curves depend on the lateral position of the AFM tip with respect to the mica surface lattice, suggesting that the heterogeneous distribution of water molecules on a solid surface can be detected using adequate experimental techniques.

In this study, we employed massive all-atom molecular dynamics simulations to mimic a capped carbon nanotube (CNT) tip that may be used as an AFM probe for the measurement of hydration forces at the alumina−water interface. The surface chosen for our simulations is alumina. The surface chemistry of crystalline and amorphous Al_2O_3 under various conditions has been extensively investigated both experimentally and theoretically.[33−38] It has been observed experimentally that in a dry environment the (0001) α-Al_2O_3 surface can terminate with an aluminum layer.[33] In agreement, Garofalini and co-workers predicted, using theoretical arguments, that the most energetically stable termination for aluminum oxide is the aluminum terminated.[39] In humid environments, complex surface hydroxylation and dehydroxylation phenomena occur.[40−46] For instance, Eng *et al.* reported experimental evidence for an oxygen-terminated surface and also for the formation of an ordered layer of contact water on the hydrated α-Al_2O_3 (0001) surface.[47] An experimental investigation by Coustet *et al.* confirms a well-defined surface hydroxylation on α-Al_2O_3 surfaces, in which the oxygen atoms are strongly coordinated with interfacial water.[48] An *ab initio* molecular dynamics study by Hass *et al.* revealed that the first atomic layer on a highly reactive Al-terminated α-alumina (0001) surface, at high water coverage, is likely to be etched away, yielding a completely hydroxylated surface.[49] Several AFM studies have been conducted for imaging metal oxide surfaces, including α-Al_2O_3. These studies provided results consistent with various surface terminations.[50,51] For example, recent contact-mode AFM results by Gan *et al.* revealed atomic-scale features on the (0001) α-Al_2O_3 surface in water, suggesting O-termination, consistent with a fully hydroxylated surface.[52]

RESULTS AND DISCUSSION

Two alumina surfaces were considered for this work, both obtained from the (0001) crystallographic face of corundum α-Al_2O_3. One surface was Al-terminated and the other fully hydroxylated. The AFM tip was simulated as a capped (28,0) rigid single-walled carbon nanotube (CNT). A CNT was chosen as the AFM tip because of its well-known high aspect ratio and because prior experimental investigations employed such tips to sample hydration water structure.[53] Single-walled CNT tips have also been successfully employed by Chen *et al.* to image, *via* AFM, gold nanoclusters and DNA molecules.[54] The simulations were conducted in the presence of explicit water at 300 K. The amount of water simulated (15 000 molecules) was sufficient to yield a thin liquid film near the solid surfaces of interest, in equilibrium with its own vapor. Other simulation details and algorithms are provided in the Simulation Methods section.

To evaluate the effect of CNT on the structure of interfacial water, we calculated the forces acting on the tip as a function of its distance from the alumina surface. The results are shown in Figure 1. The average of the total force obtained from 10 to 15 Å is used to offset the data along the *y*-axis. The separation is defined as distance along the *z*-axis between the terminal carbon atom of the CNT cap and the top aluminum atomic layer and the oxygen of the hydroxyl group of the Al-terminated and hydroxylated surfaces, respectively. The force−distance data, which are in qualitative agreement with previous theoretical studies,[21,30] may be directly compared to results from AFM force spectroscopy experiments. Although experimental data for a system corresponding to the one simulated herein are not available, thus direct comparison cannot be attempted, we point out that the magnitude of the forces obtained by our simulations is comparable to that found by Fukuma *et al.* for aqueous PBS near mica surfaces (they used a silicon tip).[25] Although the measured force should be proportional to the square of the tip diameter, thus stronger forces are expected when larger tips are employed, it is

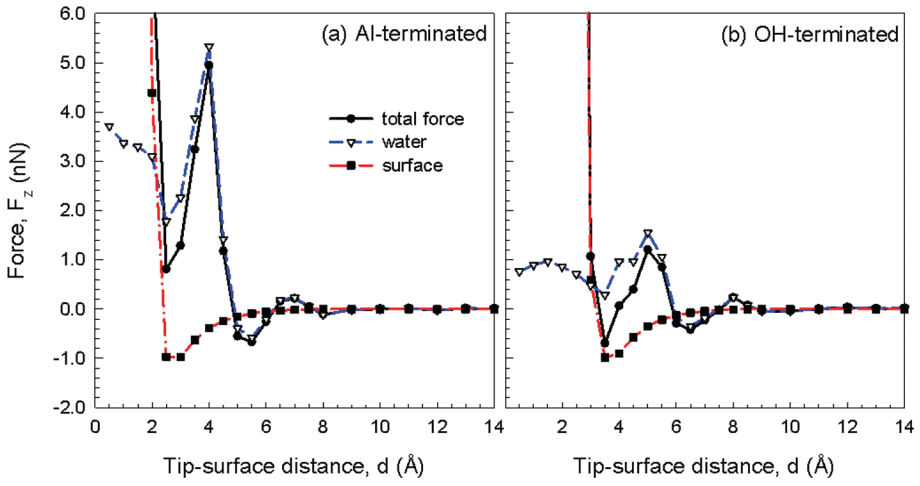

Figure 1. The *z*-component of the total force experienced by one (28,0) CNT, used as the AFM tip, as a function of the tip−surface distance in the presence of water is shown as a black curve (filled circles). The contributions due to interfacial water molecules and to the alumina surfaces are shown as blue dashed (open triangles) and red dash-dotted (filled squares) curves, respectively.

expected that as the AFM tip size increases the details in the force profiles may be overlooked. More importantly, the detailed analysis of simulation data can provide molecular insights on the features that appear in experimental AFM force−distance data. Specifically, the black solid curves shown in Figure 1a,b represent the *z*-component of the total force acting on the CNT at the Al-terminated and OH-terminated alumina surfaces, respectively. In addition, we present the components of the total force due to the solvent (water) and the solid surface (blue dashed and red dash-dotted curves, respectively).

On both surfaces, we found no significant contribution to the total force due to the alumina surface at distances greater than 6.0 Å. At smaller separations, we observe attractive alumina−CNT forces, followed by a strong repulsion when the tip comes in contact with the surface. The *z*-component of the force on the CNT due to water molecules (blue dashed curve) shows an oscillatory behavior for tip−sample distances smaller than ~9.0 Å. The width of the force oscillations is ~2.5 Å at the Al-terminated alumina surface, and a much stronger repulsive force is observed at 4.0 Å than at 7.0 Å. The different intensity of the two repulsive forces is due primarily to the differences in density observed, which correspond to first and second interfacial layers. The total force profile data obtained on the fully hydroxylated alumina surface, given in Figure 1b, show two repulsive peaks at 5.0 and 8.0 Å. The width of the first peak is ~3.0 Å. It is slightly larger than expected from the diameter of a water molecule because it includes a shoulder at ~4.0 Å. Comparing simulated force data along the shoulder shows that hydration forces do not change significantly as the separation distance decreases from 4.5 to 4.0 Å, while the tip−surface interactions become notably more attractive. Models of solvent structure that specify a Gaussian diffusion distribution for each solvent layer and reduce the width of the distribution for layers near the surface due to confinement lead to sinusoidal force profiles.[55] Our findings suggest that nonsinusoidal oscillatory forces may appear on AFM force−distance data because of changes in location and orientation experienced by interfacial water when confined between the solid substrate and the AFM tip. This observation cannot be captured by theoretical predictions unless the detailed properties of the solid substrate and the molecular features of water are taken into account, as can be done by atomistic molecular dynamics simulations.

Density changes near the tip due to the structure of the interfacial water lead to the force profiles shown in Figure 1. The water molecule oxygen atom density as a function of distance from the OH-terminated surface is shown for a few CNT−surface distances in Figure 2a. Two well-defined interfacial water layers form at the OH-terminated alumina surface. One additional pronounced layer forms around the CNT. When the CNT−surface separation is larger than ~9.0 Å, the two hydration layers on the OH-terminated α-Al_2O_3 surface form at z = 2.60 and 5.25 Å (more details available as Supporting Information S1). The hydration layer on the CNT forms at approximately 3.0 Å from the carbon atoms. As the apex of the CNT tip approaches the interfacial water, nonsinusoidal oscillatory forces are observed (see Figure 1b). The intensity and width of these oscillatory forces are directly related to the density and structural properties of the interfacial hydration layers. It is important to point out that the maxima in the force profiles are not strictly associated with the expulsion of water molecules from the region between the AFM tip and the alumina surface but are rather due to the interactions between merging interfacial water layers from the alumina−water and CNT−water interfaces. These effects are shown explicitly in the density profiles of Figure 2a, obtained at

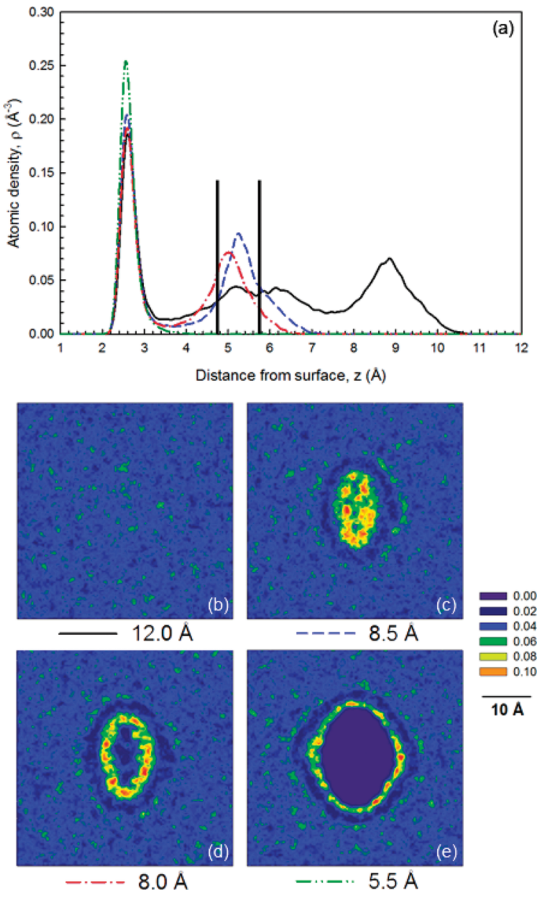

Figure 2. (a) Atomic density profiles of water oxygen as a function of the distance *z* perpendicular to the OH-terminated alumina surface for tip−surface distances at 12.0, 8.5, 8.0, and 5.5 Å are shown in solid black, dashed blue, dash-dotted red, and dash-double-dotted green curves, respectively. The two vertical black lines highlight the second hydration layer, whose density and position change as the CNT tip approaches the surface. (b−e) The *x*−*y* planar density distributions of the second interfacial water layer at 5.25 Å for the four tip−surface distances.

four different tip−surface separation distances. Note that as the tip approaches the surface, the peak located closest to the surface shows only changes in intensity. Both peak position and intensity change for the second hydration layer near the OH-terminated surface for different tip−surface separation distances.

To further investigate the AFM effects on the second hydration layer, we computed in-plane density distributions for interfacial water molecules. The results, shown in Figure 2b−e, are calculated within *x*−*y* planes parallel to the solid substrate, of thickness d_z = 1 Å, and centered at 5.25 Å from the OH-terminated surface. This distance corresponds to the position of the second hydration peak on the OH-terminated surface when the AFM tip is far from the surface. The black vertical lines in Figure 2a delimit the region used to calculate in-plane density profiles. Data in Figure 2b illustrate a uniform distribution of water along the *x*−*y* plane when the tip−surface distance is 12.0 Å. The water density distribution changes dramatically when the tip−surface distance is 8.5 Å (Figure 2c) due to a significant increase in the local water density due to merging of the second hydration layer on the OH-terminated surface and the hydration shell on the CNT tip. When the tip−surface distance decreases from 8.5 to 8.0 Å, a simultaneous decrease in peak density and a displacement of the peak position toward the surface is observed. The in-plane water density distribution (Figure 2d) provides evidence of a ring-like structure, suggesting that the CNT, external to the hydration layer, significantly perturbs the structure of interfacial water. Because at a tip−surface separation distance of 8.0 Å our force profile (Figure 1b) indicates a pronounced repulsive peak, comparing the results in Figure 1b to those in Figure 2d suggests that the strong repulsive force is related to the interaction between the CNT tip and the hydration layer. When the CNT tip is located at 5.5 Å from the surface, it has completely penetrated the hydration layer originally found at 5.25 Å. The correspondent in-plane density profile (Figure 2e) illustrates the exclusion of water from the central region, where the CNT is, and the formation of a hydration layer around the CNT perimeter. Further detailed analysis concerning interfacial water density changes on both Al-terminated and OH-terminated alumina surfaces as a function of the CNT−surface separation is discussed in Supporting Information S1. We provide complementary density distributions along planes perpendicular to the solid substrate and passing through the CNT axis in Supporting Information S2. Collectively, our results demonstrate that the increase/decrease in water density within the hydration layers as the CNT approaches the substrate is responsible for the oscillatory forces shown in Figure 1.

To highlight the effect of the CNT tip on the structural properties of water, we calculated the density of two interfacial water layers near the alumina surface as a function of CNT−surface distance. At CNT−alumina separations greater than ∼10.0 Å, we note statistically minimal variations on the density of interfacial water layers, suggesting that disruption of the hydration layer structure only happens at close separation from a solid substrate, in agreement with a number of previous reports.[10,12,56] The first two density maxima on Al-terminated and OH-terminated surfaces are located at 5.0 and 7.5 Å, and 5.5 and 8.5 Å, respectively (details in Supporting Information S1). The positions of these peaks change as the CNT approaches the two surfaces but remain within 0.5 Å of the peak positions observed in absence of the CNT.

In Figure 3, we report the intensity of the density peaks (first and second on both surfaces) as a function of the CNT−surface separation distance. The results, shown for the Al-terminated (Figure 3a) and OH-terminated surfaces (Figure 3b), clearly demonstrate that the local water density strongly depends on the tip

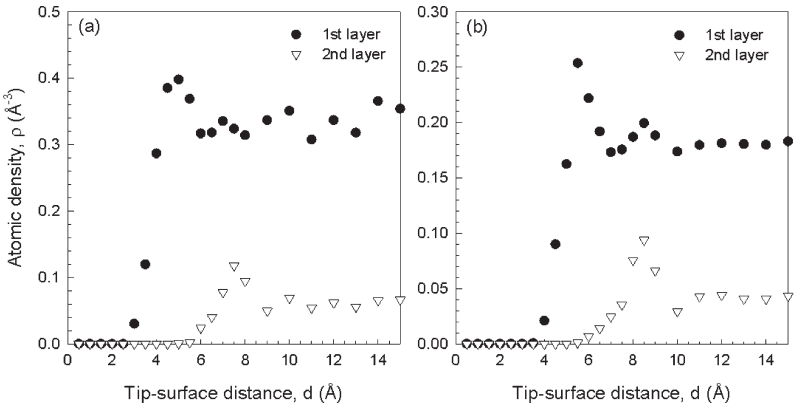

Figure 3. (a) Peak density of hydration layers located at 1.90 (solid circles) and 4.55 Å (empty triangles) at the Al-terminated alumina shown as a function of tip−surface distance. (b) Peak density of hydration layers at 2.60 and 5.25 Å at the OH-terminated alumina.

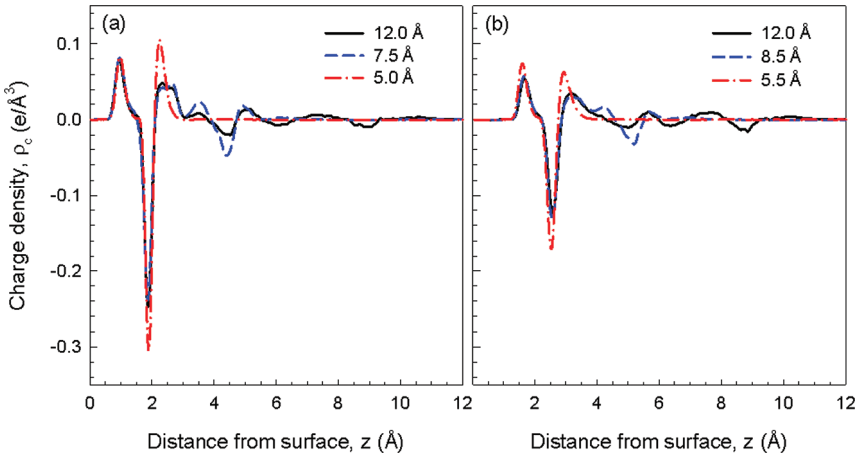

Figure 4. Charge density profiles of water as a function of the distance *z* from Al-terminated (a) and OH-terminated (b) α-Al_2O_3 surfaces. The reference *z* = 0 is the plane of aluminum and hydroxyl group oxygen atoms of the corresponding surface. Continuous, dotted, and dashed lines correspond to different CNT−surface separations.

position. It is important to point out that the CNT−surface separation distances at which the local density reaches maximum values do not necessarily correspond to CNT−surface separations at which the force profiles show maxima. For example, the density of the second hydration layer on the OH-terminated surface is maximum at a CNT−surface separation distance of 8.5 Å, while the local maximum in the correspondent force profile (Figure 1b) is observed at 8.0 Å. The changes in density at the maxima, as well as changes in their position, show that although interfacial water density is responsible for the oscillatory hydration forces shown in Figure 1, the details of the measured force profiles are due to merging of hydration layers, as well as to the orientation of interfacial water (discussed later). Further, our results show that the AFM tip affects the structure of interfacial water as it approaches the surface. Thus we argue that richer information regarding the properties of hydration water could be extracted from experimental AFM data when such data are coupled to detailed all-atom simulation studies such as those reported herein.

As observed on silica surfaces,[12] we expect that changing the degree of hydroxylation in alumina affects not only the density distribution of interfacial water but also its orientation. It is likely that both water local density and orientation affect CNT−surface interactions. To assess the orientation of interfacial water, we calculated charge density profiles at specific CNT−alumina separations. The results are presented in Figure 4a,b for Al-terminated and OH-terminated alumina surface, respectively. The data give a qualitative description of the orientation of water molecules as a function of distance from the solid substrate. Positive and negative peaks are due to contributions from water hydrogen and oxygen atoms, respectively, as they organize in layers. In regions where water has little or no preferential orientation, the charge density values are close to zero. The data indicate a distinct preferential orientation for water molecules at the interface at the two alumina substrates. For instance, water molecules in the first layer have a hydrogen-down orientation on both surfaces. Because, as shown in detail elsewhere,[10] the orientation of water

molecules near a solid surface yields hydrogen-bonding networks that affect the properties, including the local density, of water molecules further from the surface, changes in the orientation of interfacial water molecules can yield different hydration forces.

When the CNT is close to the surface, the orientation of the interfacial water becomes important. The data presented in Figure 4a for the Al-terminated surface (5.0 Å, red dotted line) indicate that the tip approaching the surface (black line to red dotted line) causes an increase of the charge density consistent with an increasing atomic hydrogen density near 2.3 Å, which means some of the water molecules present in the first hydration layer at 1.9 Å have a pronounced hydrogen-up orientation. The data presented for the OH-terminated surface, in Figure 4b, illustrate a similar behavior for water in the first interfacial layer. For the OH-terminated surface, when the CNT is at 5.5 Å, both positive and negative peaks in the charge density increase. The different response of interfacial water on the Al-terminated and OH-terminated alumina to the approaching CNT tip suggests that force spectroscopy experiments might be very sensitive to local changes in the chemical nature of the solid substrate. The contribution of the molecular orientation, typically overlooked because of secondary importance to the effect of local water density, contributes to explain the effects of heterogeneous surface charge distributions on hydration forces.

In summary, we conducted massive all-atom molecular dynamics simulations to interpret hypothetical experimental data that could be obtained when an AFM with a carbon nanotube tip (CNT) is used to sample the structure of interfacial water on an atomically smooth α-Al_2O_3 surface. Aluminum and hydroxyl terminations of the alumina surfaces were considered to assess the effect of the surface chemistry on the forces acting on the AFM tip. A capped (28,0) single-walled CNT was considered as the AFM tip. A number of independent simulations were conducted at ambient conditions for various tip−surface separations to reconstruct the force profile. The results suggest that oscillatory forces act on the CNT at small separations (less than 10 Å). Both intensity and width (~2.5−3.0 Å) of the oscillations are primarily due to significant changes on local water density and molecular orientation at the alumina interface due to the CNT. Local density increases yield pronounced repulsive forces, while local density depletions yield less repulsive forces, which in some circumstances may become attractive, depending on the system considered. However, the maxima and minima in the force profiles do not necessarily correspond to the position of the hydration layers. The orientation of interfacial water, which affects the hydrogen-bonding network between interfacial water molecules, modulates the hydration forces, although to a smaller extent compared to local water density.

CONCLUSIONS

In this paper, we presented results from massive all-atom molecular dynamics simulations to reproduce a hypothetical AFM experiment conducted to sample the structure of hydration layers near an alumina substrate. The AFM tip was modeled as a rigid single-walled carbon nanotube. Because the features of the force profiles are always related to the behavior of the water molecules confined between the CNT tip and the alumina surface, changes in the surface termination, which affect both structure and orientation of interfacial water, most likely lead to markedly different force profiles in terms of both intensity of repulsive force and periodicity of oscillatory forces. On the basis of our results, experimental force spectroscopy analysis should be able to sample and differentiate between hydration forces observed on materials characterized by heterogeneous properties. By coupling experimental AFM studies to detailed theoretical insights such as those provided by all-atom simulations, it will be possible to correctly interpret the structure and properties of hydration water, offering the possibility of leaps forward in a number of nanotechnological applications, such as the design of nanofluidic devices.

SIMULATION METHODS

The (0001) crystallographic face of corundum α-Al_2O_3 (space group $R\bar{3}$)[57] was used to model the alumina solid substrate according to the CLAYFF force field.[58] Two fully flexible (0001) α-Al_2O_3 surfaces were considered. One Al-terminated and one OH-terminated (fully hydroxylated surface with ~15 OH/nm^2) alumina surfaces were employed to assess water properties under different surface chemistry conditions. Each of the surfaces was placed at the bottom of one simulation box. The *x* and *y* dimensions of the solid substrate were both approximately 90.5 Å in length, for a total surface area of ~82 nm^2. The thickness of the Al-terminated and OH-terminated alumina surfaces was 12.75 and 12.10 Å along the *z*-axis, respectively. Fifteen thousand water molecules were simulated on the surface, sufficient to yield a thin liquid film. A rigid (28,0) capped single-walled CNT of 10.0 nm length was positioned perpendicular to the solid substrate at a fixed separation. The *z* dimension of the simulation box is 16.27 nm in all cases. Periodic boundary conditions are implemented in all three directions. At the conditions chosen, the chemical potential of water remains constant independently on the nanotube−surface distance, which is consistent with the experiments we seek to reproduce. Interactions between the CNT tip and the alumina surface were excluded during our simulations since the CNT was fixed and the changes on the alumina structure due to the CNT were out of the scope of this work. In Figure 5, we report a simulation snapshot for the entire simulation system.

The carbon atoms of the CNT were modeled as Lennard-Jones (LJ) spheres using the parameters proposed by Cheng and Steele[59] and kept rigid during the simulations. The SPC/E model was used to describe water. This model is known to reproduce well structure and dynamics of bulk water.[60] The bonds and angles of water molecules were kept fixed by

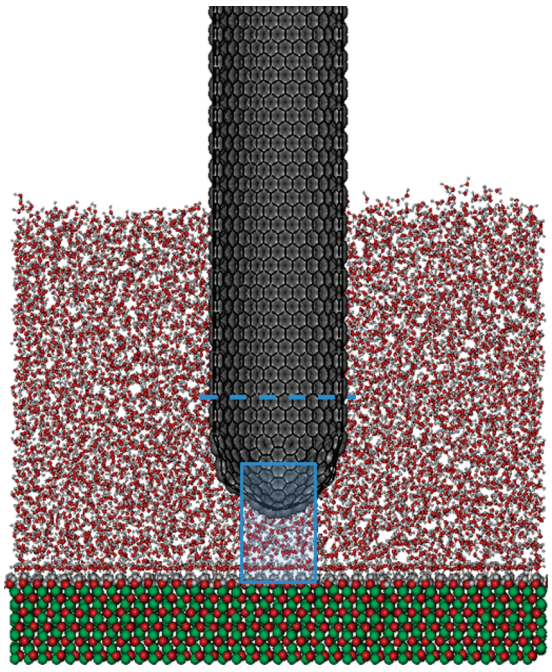

Figure 5. Cross-sectional view of one flat alumina substrate, the CNT, and water molecules considered in our simulations. Aluminum, oxygen, and hydrogen atoms of the fully hydroxylated alumina surface are shown as green, red, and white spheres, respectively. Carbon atoms are shown in dark gray. Water molecules are represented by red (oxygen) and white (hydrogen) spheres. The carbon atoms considered for the force calculation of Figure 1 are those below the blue dashed line. The snapshot also provides a side view of the cylindrical volume considered for the calculation of atomic and charge densities (blue box below the CNT tip).

employing the SETTLE algorithm.[61] Nonbonded interactions were modeled by means of dispersive and electrostatic forces. The electrostatic interactions were modeled by a Coulombic potential. The dispersive interactions were modeled with a 12−6 LJ potential. The LJ parameters for unlike interactions were determined by Lorentz−Berthelot mixing rules.[62] The cutoff distance for all interactions was 9 Å, and long-range electrostatic interactions were treated using the particle mesh Ewald (PME) method.[63]

All simulations were performed in the canonical ensemble where the number of particles, the simulation volume, and the temperature (*T*) were kept constant. The system temperature was fixed at 300 K and controlled by a Nosé-Hoover thermostat[64,65] with a relaxation time of 100 fs.

We performed 24 independent simulations for each of the two alumina surfaces at decreasing separation, from 15 to 0.5 Å, between the CNT and the solid substrate. At the furthest distance, the CNT was located 15 Å away from the substrate. The decrement in the separation distance for the first 7 simulations was 1 Å; 0.5 Å for the remaining ones. The closest tip−surface separation corresponds to contact. In all cases, 15 000 water molecules were simulated to create a thin water film in contact with the solid surface. Approximately 50% of the 10 nm long CNT was immersed in water.

The equations of motion were integrated with the simulation package GROMACS[66,67] by using the leapfrog algorithm[68] and a 1.0 fs time step. The data analysis was performed for 1 ns of production phase, conducted after 3 ns of equilibration.

The actual speed at which an AFM tip approaches the solid substrate in an experimental setup cannot be reproduced in our molecular dynamics simulations and thus employed independent simulations for a range of fixed separations. The simulation time is sufficient for water equilibration at the alumina surface and the CNT, and analysis can provide equilibrium properties for the calculation of solvation forces.

For the calculation of the forces acting on the tip, we considered the forces on the carbon atoms within the lowest 20% of the CNT length (closest to the alumina surface). In Figure 5, we report a schematic showing the carbon atoms considered. In Figure 1, we reported the ensemble average sum of the *z*-component forces acting on the various carbon atoms as a function of the CNT−surface distance. Forces due to surface atoms and water molecules are considered, while those due to the carbon atoms of CNTs are not accounted for.

Because understanding how the local water density changes in the region between the approaching CNT and the solid substrate is critical for the characterization of hydration forces, a cylindrical volume with ∼11 Å diameter parallel to the CNT and centered on the CNT axis was considered for interfacial water density and orientation calculations. A schematic showing the cylindrical volume used for density and charge density calculations is represented in Figure 5. The approach implemented allows us to quantify local changes of water structure around the CNT tip without obscuring results with data from the broader interfacial region.

Acknowledgment. Financial support was provided, in part, by the Office of Basic Energy Sciences, U.S. Department of Energy, by Contract No. DE-SC0001902 to the University of Oklahoma. Generous allocations of computing time were provided by the OU Supercomputing Center for Education and Research (OSCER) at the University of Oklahoma and by the National Energy Research Scientific Computing Center (NERSC) at Lawrence Berkeley National Laboratory. Work at the Molecular Foundry was supported by the Office of Science, Office of Basic Energy Sciences, of the U.S. Department of Energy under Contract No. DE-AC02-05CH11231.

Supporting Information Available: Water density profiles between the AFM tip (CNT) and the surface are provided as a function of tip−surface separations as Supporting Information S1. Planar water density profiles across the CNT axis are provided as Supporting Information S2. This material is available free of charge *via* the Internet at http://pubs.acs.org.

REFERENCES AND NOTES

1. Jiang, Y.; Lee, A.; Chen, J.; Cadene, M.; Chait, B. T.; MacKinnon, R. Crystal Structure and Mechanism of a Calcium-Gated Potassium Channel. *Nature* **2002,** *417*, 515–522.
2. Hille, B. *Ion Channels of Excitable Membranes*; Sinauer Associates Inc.: Sunderland, MA, 2001.
3. Fornasiero, F.; Park, H. G.; Holt, J. K.; Stadermann, M.; Grigoropoulos, C. P.; Noy, A.; Bakajin, O. Ion Exclusion by Sub-2-nm Carbon Nanotube Pores. *Proc. Natl. Acad. Sci. U.S.A.* **2008,** *105*, 17250–17255.
4. Kerisit, S.; Liu, C. X. Molecular Simulations of Water and Ion Diffusion in Nanosized Mineral Fractures. *Environ. Sci. Technol.* **2009,** *43*, 777–782.
5. Argyris, D.; Cole, D. R.; Striolo, A. Ion-Specific Effects under Confinement: The Role of Interfacial Water. *ACS Nano* **2010,** *4*, 2035–2042.
6. Malikova, N.; Cadene, A.; Marry, V.; Dubois, E.; Turq, P. Diffusion of Water in Clays on the Microscopic Scale: Modeling and Experiment. *J. Phys. Chem. B* **2006,** *110*, 3206–3214.
7. Mamontov, E.; Wesolowski, D. J.; Vlcek, L.; Cummings, P. T.; Rosenqvist, J.; Wang, W.; Cole, D. R. Dynamics of Hydration Water on Rutile Studied by Backscattering Neutron Spectroscopy and Molecular Dynamics Simulation. *J. Phys. Chem. C* **2008,** *112*, 12334–12341.
8. Fenn, E. E.; Wong, D. B.; Fayer, M. D. Water Dynamics at Neutral and Ionic Interfaces. *Proc. Natl. Acad. Sci. U.S.A.* **2009,** *106*, 15243–15248.
9. Kerisit, S.; Liu, C. X.; Ilton, E. S. Molecular Dynamics Simulations of the Orthoclase (001)- and (010)-Water Interfaces. *Geochim. Cosmochim. Acta* **2008,** *72*, 1481–1497.
10. Argyris, D.; Tummala, N. R.; Striolo, A.; Cole, D. R. Molecular Structure and Dynamics in Thin Water Films at the Silica and Graphite Surfaces. *J. Phys. Chem. C* **2008,** *112*, 13587–13599.

11. Giovambattista, N.; Rossky, P. J.; Debenedetti, P. G. Effect of Temperature on the Structure and Phase Behavior of Water Confined by Hydrophobic, Hydrophilic, and Heterogeneous Surfaces. *J. Phys. Chem. B* **2009,** *113*, 13723–13734.
12. Argyris, D.; Cole, D. R.; Striolo, A. Hydration Structure on Crystalline Silica Substrates. *Langmuir* **2009,** *25*, 8025–8035.
13. Wang, J. W.; Kalinichev, A. G.; Kirkpatrick, R. J. Asymmetric Hydrogen Bonding and Orientational Ordering of Water at Hydrophobic and Hydrophilic Surfaces: A Comparison of Water/Vapor, Water/Talc, and Water/Mica Interfaces. *J. Phys. Chem. C* **2009,** *113*, 11077–11085.
14. Kalra, A.; Garde, S.; Hummer, G. Osmotic Water Transport through Carbon Nanotube Membranes. *Proc. Natl. Acad. Sci. U.S.A.* **2003,** *100*, 10175–10180.
15. Argyris, D.; Cole, D. R.; Striolo, A. Dynamic Behavior of Interfacial Water at the Silica Surface. *J. Phys. Chem. C* **2009,** *113*, 19591–19600.
16. Gordillo, M. C.; Marti, J. Effect of Surface Roughness on the Static and Dynamic Properties of Water Adsorbed on Graphene. *J. Phys. Chem. B* **2010,** *114*, 4583–4589.
17. Mamontov, E.; Vlcek, L.; Wesolowski, D. J.; Cummings, P. T.; Wang, W.; Anovitz, L. M.; Rosenqvist, J.; Brown, C. M.; Sakai, V. G. Dynamics and Structure of Hydration Water on Rutile and Cassiterite Nanopowders Studied by Quasielastic Neutron Scattering and Molecular Dynamics Simulations. *J. Phys. Chem. C* **2007,** *111*, 4328–4341.
18. Shen, Y. R.; Ostroverkhov, V. Sum-Frequency Vibrational Spectroscopy on Water Interfaces: Polar Orientation of Water Molecules at Interfaces. *Chem. Rev.* **2006,** *106*, 1140–1154.
19. Israelachvili, J. Solvation Forces and Liquid Structure, as Probed by Direct Force Measurements. *Acc. Chem. Res.* **1987,** *20*, 415–421.
20. Jarvis, S. P.; Uchihashi, T.; Ishida, T.; Tokumoto, H.; Nakayama, Y. Local Solvation Shell Measurement in Water Using a Carbon Nanotube Probe. *J. Phys. Chem. B* **2000,** *104*, 6091–6094.
21. Li, T. D.; Gao, J. P.; Szoszkiewicz, R.; Landman, U.; Riedo, E. Structured and Viscous Water in Subnanometer Gaps. *Phys. Rev. B* **2007,** *75*, 115415.
22. Kimura, K.; Ido, S.; Oyabu, N.; Kobayashi, K.; Hirata, Y.; Imai, T.; Yamada, H. Visualizing Water Molecule Distribution by Atomic Force Microscopy. *J. Chem. Phys.* **2010,** *132*, 194705.
23. Higgins, M. J.; Polcik, M.; Fukuma, T.; Sader, J. E.; Nakayama, Y.; Jarvis, S. P. Structured Water Layers Adjacent to Biological Membranes. *Biophys. J.* **2006,** *91*, 2532–2542.
24. Loh, S. H.; Jarvis, S. P. Visualization of Ion Distribution at the Mica−Electrolyte Interface. *Langmuir* **2010,** *26*, 9176–9178.
25. Fukuma, T.; Ueda, Y.; Yoshioka, S.; Asakawa, H. Atomic-Scale Distribution of Water Molecules at the Mica−Water Interface Visualized by Three-Dimensional Scanning Force Microscopy. *Phys. Rev. Lett.* **2010,** *104*, 016101-10.
26. O'Shea, S. J. Oscillatory Forces in Liquid Atomic Force Microscopy. *Jpn. J. Appl. Phys., Part 1* **2001,** *40*, 4309–4313.
27. Hayes, R.; Warr, G. G.; Atkin, R. At the Interface: Solvation and Designing Ionic Liquids. *Phys. Chem. Chem. Phys.* **2010,** *12*, 1709–1723.
28. Fukuma, T.; Higgins, M. J.; Jarvis, S. P. Direct Imaging of Individual Intrinsic Hydration Layers on Lipid Bilayers at Angstrom Resolution. *Biophys. J.* **2007,** *92*, 3603–3609.
29. Fukuma, T.; Kobayashi, K.; Matsushige, K.; Yamada, H. True Molecular Resolution in Liquid by Frequency-Modulation Atomic Force Microscopy. *Appl. Phys. Lett.* **2005,** *86*, 193108-3.
30. Patrick, D. L.; Lynden-Bell, R. M. Atomistic Simulations of Fluid Structure and Solvation Forces in Atomic Force Microscopy. *Surf. Sci.* **1997,** *380*, 224–244.
31. Ho, R. Y.; Yuan, J. Y.; Shao, Z. F. Hydration Force in the Atomic Force Microscope: A Computational Study. *Biophys. J.* **1998,** *75*, 1076–1083.
32. Hiasa, T.; Kimura, K.; Onishi, H.; Ohta, M.; Watanabe, K.; Kokawa, R.; Oyabu, N.; Kobayashi, K.; Yamada, H. Aqueous Solution Structure over α-Al_2O_3(0112) Probed by Frequency-Modulation Atomic Force Microscopy. *J. Phys. Chem. C* **2010,** *114*, 21423–21426.
33. Ahn, J.; Rabalais, J. W. Composition and Structure of the Al_2O_3 {0001}-(1 × 1) Surface. *Surf. Sci.* **1997,** *388*, 121–131.
34. Nygren, M. A.; Gay, D. H.; Catlow, C. R. A. Hydroxylation of the Surface of the Corundum Basal Plane. *Surf. Sci.* **1997,** *380*, 113–123.
35. Blonski, S.; Garofalini, S. H. Molecular Dynamics Study of Silica−Alumina Interfaces. *J. Phys. Chem.* **1996,** *100*, 2201–2205.
36. Adiga, S. P.; Zapol, P.; Curtiss, L. A. Atomistic Simulations of Amorphous Alumina Surfaces. *Phys. Rev. B* **2006,** *74*, 064204.
37. Hinnemann, B.; Carter, E. A. Adsorption of Al, O, Hf, Y, Pt, and S Atoms on α-Al_2O_3(0001). *J. Phys. Chem. C* **2007,** *111*, 7105–7126.
38. Adiga, S. P.; Zapol, P.; Curtiss, L. A. Structure and Morphology of Hydroxylated Amorphous Alumina Surfaces. *J. Phys. Chem. C* **2007,** *111*, 7422–7429.
39. Blonski, S.; Garofalini, S. H. Molecular-Dynamics Simulations of α-Alumina and γ-Alumina Surfaces. *Surf. Sci.* **1993,** *295*, 263–274.
40. Catalano, J. G.; Park, C.; Zhang, Z.; Fenter, P. Termination and Water Adsorption at the α-Al_2O_3 (012)−Aqueous Solution Interface. *Langmuir* **2006,** *22*, 4668–4673.
41. Catalano, J. G. Relaxations and Interfacial Water Ordering at the Corundum (110) Surface. *J. Phys. Chem. C* **2010,** *114*, 6624–6630.
42. Wittbrodt, J. M.; Hase, W. L.; Schlegel, H. B. *Ab Initio* Study of the Interaction of Water with Cluster Models of the Aluminum Terminated (0001) α-Aluminum Oxide Surface. *J. Phys. Chem. B* **1998,** *102*, 6539–6548.
43. Hass, K. C.; Schneider, W. F.; Curioni, A.; Andreoni, W. The Chemistry of Water on Alumina Surfaces: Reaction Dynamics from First Principles. *Science* **1998,** *282*, 265–268.
44. Shapovalov, V.; Truong, T. N. *Ab Initio* Study of Water Adsorption on α-Al_2O_3 (0001) Crystal Surface. *J. Phys. Chem. B* **2000,** *104*, 9859–9863.
45. Wang, X. G.; Chaka, A.; Scheffler, M. Effect of the Environment on α-Al_2O_3 (0001) Surface Structures. *Phys. Rev. Lett.* **2000,** *84*, 3650–3653.
46. Lodziana, Z.; Norskov, J. K.; Stoltze, P. The Stability of the Hydroxylated (0001) Surface of α-Al_2O_3. *J. Chem. Phys.* **2003,** *118*, 11179–11188.
47. Eng, P. J.; Trainor, T. P.; Brown, G. E.; Waychunas, G. A.; Newville, M.; Sutton, S. R.; Rivers, M. L. Structure of the Hydrated α-Al_2O_3 (0001) Surface. *Science* **2000,** *288*, 1029–1033.
48. Coustet, V.; Jupille, J. High-Resolution Electron-Energy-Loss Spectroscopy of Isolated Hydroxyl-Groups on α-Al_2O_3 (0001). *Surf. Sci.* **1994,** *309*, 1161–1165.
49. Hass, K. C.; Schneider, W. F.; Curioni, A.; Andreoni, W. First-Principles Molecular Dynamics Simulations of H_2O on α-Al_2O_3 (0001). *J. Phys. Chem. B* **2000,** *104*, 5527–5540.
50. Barth, C.; Reichling, M. Imaging the Atomic Arrangements on the High-Temperature Reconstructed α-Al_2O_3 (0001) Surface. *Nature* **2001,** *414*, 54–57.
51. Lauritsen, J. V.; Reichling, M. Atomic Resolution Non-Contact Atomic Force Microscopy of Clean Metal Oxide Surfaces. *J. Phys.: Condens. Matter* **2010,** *22*, 263001.
52. Gan, Y.; Franks, G. V. High Resolution AFM Images of the Single-Crystal α-Al_2O_3 (0001) Surface in Water. *J. Phys. Chem. B* **2005,** *109*, 12474–12479.
53. Katan, A. J.; Oosterkamp, T. H. Measuring Hydrophobic Interactions with Three-Dimensional Nanometer Resolution. *J. Phys. Chem. C* **2008,** *112*, 9769–9776.
54. Chen, L. W.; Cheung, C. L.; Ashby, P. D.; Lieber, C. M. Single-Walled Carbon Nanotube AFM Probes: Optimal Imaging Resolution of Nanoclusters and Biomolecules in Ambient and Fluid Environments. *Nano Lett.* **2004,** *4*, 1725–1731.

55. Ashby, P. D.; Lieber, C. M. Brownian Force Profile Reconstruction of Interfacial 1-Nonanol Solvent Structure. *J. Am. Chem. Soc.* **2004,** *126*, 16973–16980.
56. Marti, J.; Sala, J.; Guardia, E. Molecular Dynamics Simulations of Water Confined in Graphene Nanochannels: From Ambient to Supercritical Environments. *J. Mol. Liq.* **2010,** *153*, 72–78.
57. Többens, D. M.; Stüsser, N.; Knorr, K.; Mayer, H. M.; Lampert, G. E9: The New High-Resolution Neutron Powder Diffractometer at the Berlin Neutron Scattering Center. *Mater. Sci. Forum* **2001,** *378−3*, 288–293.
58. Cygan, R. T.; Liang, J.-J.; Kalinichev, A. G. Molecular Models of Hydroxide, Oxyhydroxide, and Clay Phases and the Development of a General Force Field. *J. Phys. Chem. B* **2004,** *108*, 1255–1266.
59. Cheng, A.; Steele, W. A. Computer-Simulation of Ammonia on Graphite.1. Low-Temperature Structure of Monolayer and Bilayer Films. *J. Chem. Phys.* **1990,** *92*, 3858–3866.
60. Berendsen, H. J. C.; Grigera, J. R.; Straatsma, T. P. The Missing Term in Effective Pair Potentials. *J. Phys. Chem.* **1987,** *91*, 6269–6271.
61. Miyamoto, S.; Kollman, P. A. SETTLE: An Analytical Version of the Shake and Rattle Algorithm for Rigid Water Models. *J. Comput. Chem.* **1992,** *13*, 952–962.
62. Allen, M. P.; Tildesley, D. J. *Computer Simulation of Liquids*; Oxford University Press: Oxford, 2004.
63. Essmann, U.; Perera, L.; Berkowitz, M. L.; Darden, T.; Lee, H.; Pedersen, L. G. A Smooth Particle Mesh Ewald Method. *J. Chem. Phys.* **1995,** *103*, 8577.
64. Nose, S. A Molecular-Dynamics Method for Simulations in the Canonical Ensemble. *Mol. Phys.* **1984,** *52*, 255–268.
65. Hoover, W. G. Canonical Dynamics: Equilibrium Phase-Space Distributions. *Phys. Rev. A* **1985,** *31*, 1695–1697.
66. van der Spoel, D.; Lindahl, E.; Hess, B.; Groenhof, G.; Mark, A. E.; Berendsen, H. J. C. Gromacs: Fast, Flexible, and Free. *J. Comput. Chem.* **2005,** *26*, 1701–1718.
67. Hess, B.; Kutzner, C.; vanderSpoel, D.; Lindahl, E. Gromacs 4: Algorithms for Highly Efficient, Load-Balanced, and Scalable Molecular Simulation. *J. Chem. Theory Comput.* **2008,** *4*, 435–447.
68. Hockney, R. W.; Goel, S. P.; Eastwood, J. W. Quiet High-Resolution Computer Models of a Plasma. *J. Comput. Phys.* **1974,** *14*, 148–158.